Development 134, 3191-3201 (2007) doi:10.1242/dev.005884

Mice lacking sister chromatid cohesion protein PDS5B exhibit developmental abnormalities reminiscent of Cornelia de Lange syndrome

Bin Zhang[1,2], Sanjay Jain[3], Haengseok Song[2], Ming Fu[4,5], Robert O. Heuckeroth[4,5], Jonathan M. Erlich[5], Patrick Y. Jay[1,5] and Jeffrey Milbrandt[2,6,*]

PDS5B is a sister chromatid cohesion protein that is crucial for faithful segregation of duplicated chromosomes in lower organisms. Mutations in cohesion proteins are associated with the developmental disorder Cornelia de Lange syndrome (CdLS) in humans. To delineate the physiological roles of PDS5B in mammals, we generated mice lacking PDS5B (APRIN). *Pds5B*-deficient mice died shortly after birth. They exhibited multiple congenital anomalies, including heart defects, cleft palate, fusion of the ribs, short limbs, distal colon aganglionosis, abnormal migration and axonal projections of sympathetic neurons, and germ cell depletion, many of which are similar to abnormalities found in humans with CdLS. Unexpectedly, we found no cohesion defects in *Pds5B*$^{-/-}$ cells and detected high PDS5B expression in post-mitotic neurons in the brain. These results, along with the developmental anomalies of *Pds5B*$^{-/-}$ mice, the presence of a DNA-binding domain in PDS5B in vertebrates and its nucleolar localization, suggest that PDS5B and the cohesin complex have important functions beyond their role in chromosomal dynamics.

KEY WORDS: PDS5, APRIN, Sister chromatid cohesion, Congenital defects, Cornelia de Lange syndrome, Primordial germ cells, Mouse

INTRODUCTION

Sister chromatid cohesion, the linkage of sister chromatids from S phase until onset of anaphase, is important for accurate chromosome segregation during cell division and is mediated by a highly conserved multi-protein complex, called cohesin. The cohesin complex consists of core components, SMC1, SMC3, SCC1 and SCC3, and cohesin activity is regulated by its regulatory factors, PDS5, SCC2, SCC4 and ECO1 (Hartman et al., 2000; Nasmyth and Haering, 2005). In addition to chromosomal dynamics, cohesin and its regulatory factors also play important roles in development. For example, *Mau-2*, a recently identified metazoan homolog of yeast *SCC4*, not only participates in sister chromatid cohesion, but also guides cell movement and axonal outgrowth during development (Benard et al., 2004; Seitan et al., 2006; Watrin et al., 2006). In *Drosophila*, mutants of cohesion factors (e.g. SMC1 and NIPPED-B) regulate transcription of *cut* and other genes encoding developmental regulators through attenuating cohesin-mediated blocking of long-range enhancer and promoter communication (Dorsett et al., 2005; Rollins et al., 2004). This additional developmental function has recently been extended to humans with the discovery that mutations in *NIPBL*, *SMC1A* and *SMC3* are responsible for ~50% of cases of Cornelia de Lange syndrome (CdLS). CdLS patients present with a variety of developmental anomalies, including dysmorphic facial features, mental retardation, growth delay, limb reduction, genital anomalies and cardiac defects (Deardorff et al., 2007; Krantz et al., 2004; Musio et al., 2006; Tonkin et al., 2004).

Departments of [1]Genetics, [2]Pathology and Immunology, [3]Medicine and Renal division, [4]Molecular Biology and Pharmacology, [5]Pediatrics, and [6]HOPE Center for Neurological Disorders, Washington University School of Medicine, 660 South Euclid Avenue, St Louis, MO 63110, USA.

*Author for correspondence (e-mail: jmilbrandt@wustl.edu)

Accepted 22 June 2007

PDS5 is a regulatory component of cohesin and interacts genetically or physically with the cohesion factors SCC2, ECO1, SMC1, SMC3, SCC1 and SCC3 (Losada et al., 2005; Tanaka et al., 2001) to ensure proper sister chromatid cohesion during mitosis and meiosis (Hartman et al., 2000; Panizza et al., 2000; van Heemst et al., 1999). The N-terminal region of PDS5 contains several HEAT repeats, a motif that is involved in protein-protein interactions and is present in other cohesin subunits and regulatory factors (i.e. SCC2) (Neuwald and Hirano, 2000; Panizza et al., 2000). In vertebrates, there are two homologs of *PDS5*, *PDS5A* and *PDS5B*, that both contribute to cohesion dynamics (Losada et al., 2005). Interestingly, in addition to its regulation of chromatid cohesion, PDS5 also appears to directly regulate transcription of a number of developmental genes. For example, similar to SCC2/NIPPED-B and SMC1, PDS5 regulates transcription of the *Drosophila cut* gene during wing development (Dorsett et al., 2005). In humans because *PDS5B* (also known as *APRIN* in human and mouse) is located in a region where loss of heterozygosity is commonly detected in tumors (13q12.3), it may act as a tumor suppressor (Geck et al., 2000). Furthermore, PDS5B regulates androgen-induced differentiation of prostate epithelial cells (Geck et al., 2000). Finally, lethality in yeast *Pds5* mutants can be rescued by overexpression of topoisomerase II, however, TOPII does not compensate for the cohesion deficit in these mutants, indicating that PDS5 has crucial functions in yeast beyond those related to chromosome cohesion (Aguilar et al., 2005).

To delineate physiological roles of PDS5B in mammals we generated *Pds5B*-deficient mice using homologous recombination. Loss of *Pds5B* results in a number of developmental defects, including dysmorphic facies, cleft palate, skeletal patterning and bone development defects, cardiac malformation, distal enteric nervous system (ENS) aganglionosis, abnormal autonomic nervous system formation, and depletion of primordial germ cells. Together, these results indicate that PDS5B and perhaps the cohesin complex itself is a critical regulator of multiple aspects of organogenesis. The association of CdLS with mutations in several different cohesion

proteins and the constellation of developmental defects in *Pds5B*$^{-/-}$ mice indicate the widespread role of the cohesion factors in normal development, and provide a possible mechanism for their role in the pathogenesis of CdLS and related developmental disorders. As the first mouse model resembling CdLS, the *Pds5B*-deficient mice will be useful in delineating how PDS5B and cohesin regulate developmental processes.

MATERIALS AND METHODS

Generation of *Pds5B* knockout mice

Pds5B-deficent mice were generated by homologous recombination and genotypes were determined by Southern and PCR analyses.

The *Pds5B* recombination construct encompasses genomic regions surrounding the first coding exon. A 7.9 kb 5′ arm upstream of the first coding exon of *Pds5B* containing 20 nt of 5′ UTR and a 6.3 kb 3′ arm downstream of the first coding exon of *Pds5B* were generated by PCR (See below for primer sequences) and cloned into pRS315 by yeast gap repair (Le et al., 2005). The final targeting construct was generated using yeast gap repair by co-transforming yeast with linearized 7.9 kb 5′ arm in pRS315, 6.3 kb 3′ arm in pRS315, the β-gal-PGK-Neo (β-gal-Neo) cassette, and two adapters. Two adapters were generated by annealing adapter forward and reverse primers and filled by Herculase DNA polymerase (Stratagene). For cloning the 5′ arm and 3′ arm by gap repair, pRS315 was digested with *Sac*I and *Xho*I. For cloning the final target construct, 5′ arm pRS315 and 3′ arm pRS315 were digested with *Xho*I and *Mlu*I, respectively. The final *Pds5B* recombination construct was confirmed by sequencing analysis to ensure veracity of the *Pds5B* arm regions.

The *Pds5B* targeting vector was linearized with *Kpn*I and transfected by electroporation into R1 embryonic stem cells. Homologous recombinants were screened by Southern blot hybridization using a probe downstream of the 3′ arm. Two properly targeted ES cell clones were injected into blastocysts to generate chimeric mice. The chimeras were mated and successful germline transmission of the targeted allele was detected by Southern blotting. Heterozygous mice grew normally and were mated to β-actin Cre mice to remove the PGK-Neo cassette. The phenotypes of two independent lines (before or after excision of the PGK-Neo cassette) were similar. All animal procedures were performed according to our institutional approved protocols. Experiments were performed on mice from a mixed 129Sv/B6 background. The genotypes of *Pds5B* mutant mice were determined using Southern blotting or PCR using primers P1, P2, P3 (95°C 30 seconds, 58°C 60 seconds, 72°C 90 seconds; 35 cycles). Wild-type and mutant alleles were amplified with P1-P2 (390 nt amplicon) and P1-P3 (450 nt amplicon) primer pairs, respectively. (See below for primer sequences.)

Primers, containing *Pds5B* genomic and associated *pRS315* sequences, used for PCR amplification of the 5′ arm and 3′ arm of the targeting construct were as follows:

5′ arm forward primer: TTAATGCGCCGCTACAGGGCGCGTCACGCGTCTGTGCTGGAGCTCACATGACCTGTCCT; 5′ arm reverse primer: ACAGCTATGACCATGATTACGCCAACTCGAGGATGGAAATGTCTGTACCCCTAAAGCAAGAAAA; 3′ arm forward primer: TTAATGCGCCGCTACAGGGCGCGTCACGCGTCAGTGTATGCTGCAGACAGCTGGGCAGTT; 3′ arm reverse primer: ACAGCTATGACCATGATTACGCCAACTCGAGCAGCCTGGTTTGCAGAGAGTTCTAGCACA.

Primers used to generate adapters for the final targeting construct using yeast gap repair:

Adapter 1 forward primer: GATCCCCCAAGCTTACTTAGATCTCGAGCTAGCACGCGTGATGGAAATG; adapter 1 reverse primer: TTTTCTTGCTTTAGGGGTACAGACATTTCCATCACGCGTGCTAGC. Adapter 2 forward primer: ATACATTATACGAAGTTATACCGGTTAATTAAGGGCTCGAGCTAGCGGGCCC; Adapter 2 reverse primer: CACACAAACTGCCCAGCTGTCTGCAGCATACACTGGGGCCCGCTAGCTCGAGCCCTTAA.

Primers used to genotype Pds5B mutant mice: P1, CCAGACCTGAAGAATTGGTGGAGGA; P2, ACCCTCCTGGAGTCAAGGAAA; P3, ACCCTCCTGGAGTCAAGGAAA.

Generation of polyclonal antibody against mouse PDS5B

Rabbit anti-PDS5B polyclonal antibodies were raised using C-terminal peptide immunogen NH2-CATKENDSSEEMDV-COOH (Pacific Immunology, CA, USA). The same peptide was crosslinked to a solid support by using SulfoLink coupling Gel (Pierce Biotechnology, IL, USA) and used for affinity purification of antibodies from serum.

Immunohistochemistry and western blot analysis

Tissues used in immunohistochemistry were fixed in paraformaldehyde or Bouin's fixative. For antigen retrieval, paraffin-embedded sections were de-paraffinized in xylene, hydrated and boiled in 1 mM EDTA solution for 30 minutes prior to immunostaining (Jain et al., 2004; Naughton et al., 2006). Primary antibodies used in this study include sheep tyrosine hydroxylase (TOH; Chemicon), rabbit neuron-specific class III β-tubulin (TuJ1; Covance), rat GCNA1 (George C. Enders, PhD, University of Kansas Medical Center, Kansas City, KS, USA), mouse BrdU (Roche), which were visualized using donkey anti-sheep HRP (Jackson ImmunoResearch), donkey anti-rabbit Alexa Fluor 488 (1:100; Molecular Probes), goat anti-rat Cy3 (Jackson ImmunoResearch), or goat anti-mouse Alexa Fluor 488 (Molecular Probes) secondary antibodies. Bisbenzimide (2 μg/ml; Sigma) was used for nuclear staining.

Western blot analysis was performed using standard techniques using proteins derived from embryonic day (E) 14.5 forelimbs. The limbs were lysed in 2× SDS protein lysis buffer (100 mM Tris-HCl, pH 6.8, 4% SDS, 1× protease inhibitor cocktail; Roche). The western blots were probed with rabbit anti-PDS5B antibody (1:500 dilution) and PDS5B was visualized using chemiluminescence substrate (Pierce). For a loading control, mouse anti-β-tubulin antibody (DSHB, University of Iowa, IA, USA) was also used at 1:20,000 dilution.

Histological analysis of bone and palate

Alizarin Red S and Alcian Blue staining of newborn mice was performed as previously described (Wellik and Capecchi, 2003). Briefly, newborn mice were skinned and dehydrated in 95% ethanol. They were then stained in Alcian Blue solution for 3 days, rehydrated and incubated in 1% KOH for 2 days, and stained with Alizarin Red S for 3 days. Embryonic and newborn heads were fixed in 4% paraformaldehyde at 4°C for 16 hours. The fixed heads were properly oriented in paraffin, coronal sections were prepared, sections were stained with Hematoxylin and Eosin (H&E) and examined microscopically for evidence of cleft palate.

Analysis of cardiac malformations

The thoraxes of newborn mice was fixed in 4% formaldehyde before the heart was dissected free and embedded in paraffin. Entire neonatal hearts were serially sectioned at 6 μm thickness, stained with H&E, and inspected for defects. Two people (J.M.E. and P.Y.J.) examined the set of sections from every heart under a 5× microscope objective. The two examiners independently made the same diagnosis for every heart in this study.

Peripheral nervous system analysis

For analysis of the enteric nervous system, the E12.5 or E18.5 whole gut was dissected from the mouse and fixed with 4% paraformaldehyde at 25°C for 30 minutes. After fixation, explants were washed three times in TBST (1 mM Tris, 150 mM NaCl, 0.2% Triton X-100) and blocked with 4% donkey serum in TBST (1 hour, 25°C) before incubation with primary antibody (4°C, overnight) in TBST. Primary antibody (rabbit anti-Tuj1, 1:100; Covance) staining was visualized using donkey anti-rabbit Alexa Fluor 488 (1:100; Molecular Probes) secondary antibody after washing three times with TBST (Fu et al., 2006). For cross-sectional analysis, post-natal day (P)0 gut was fixed in 4% paraformaldehyde and embedded in paraffin. Paraffin sections were stained with anti-Tuj1 (rabbit; Covance; 1:500) and visualized using goat anti-rabbit Cy3 (1:500; Jackson ImmunoResearch). P0 gut staining with acetylcholinesterase and analysis of the percentage of distal colon colonized by ENS precursors was performed as previously described (Jain et al., 2004).

The sympathetic nervous system of embryos and newborns was analyzed using whole-mount TOH immunohistochemistry as described previously (Enomoto et al., 2001).

Analysis of germ cells

Embryonic gonads were dissected, fixed in Bouin's solution overnight at 4°C, embedded in paraffin, and 6 μm sections were prepared. Primordial germ cells were examined by H&E staining, alkaline phosphatase histochemistry, or GCNA1 immunohistochemistry. For germ cell identification, anti-GCNA1 antibody (1:200, rat polyclonal) was used, whereas Sertoli cells were identified using anti-GATA4 antibody (1:200, goat Sertoli cells polyclonal; Santa Cruz Biotechnology) (Naughton et al., 2006).

For BrdU and GCNA1 double immunostaining, timed pregnant females were injected with 200 mg/kg body weight BrdU 2 hours prior to sacrifice (Jain et al., 2004). Paraffin-embedded sections of embryonic testis were incubated with BrdU primary antibody (1: 200; Roche) and visualized using goat anti-mouse immunoglobulin labeled with Alexa Fluor 488 (1:500; Molecular Probes) secondary antibody, followed by staining with GCNA1 (1:200) and goat anti-rat immunoglobulin labeled with Cy3 (1:500, Jackson ImmunoResearch). TUNEL was performed as previously described (Jain et al., 2004).

Testes transplantation

Testes from E16.5 mutant and wild-type mice were transplanted subcutaneously onto the back and/or flank of castrated 4- to 8-week-old male nude mice (Taconic No. NCRNUM, Germantown, NY, USA) as previously described (Honaramooz et al., 2002). The grafted donor testes were harvested and processed for histological evaluation at the indicated time points.

Metaphase spread analysis

Chromosome analysis was performed in the Chromosome Analysis Laboratory at University of Southern California directed by Chih-Lin Hsieh, PhD. Mouse embryonic fibroblasts from wild-type and *Pds5B* mutant mice (passage 3) were cultured in DMEM with 10% fetal bovine serum. Chromosomes were harvested the day after plating after growth for 1 hour in colcemid (1 μg/ml) using standard hypotonic (0.075 M KCl) treatment and fixed in methanol:acetic acid (3:1). Slides were prepared and chromosomes were analyzed using the Geimsa-trypsin-Wrights (GTW) banding method. Two cells were fully analyzed from each line, and all were found to have normal karyotypes. Twenty-two to 25 cells were examined for precocious sister chromatid separation (PSCS). To avoid selection bias, the first 22-25 metaphases encountered were included in the analysis regardless of the length of the chromosomes or differences in the quality of banding.

In situ hybridization

Mouse cDNA fragments corresponding to *Pds5B* (probe 1: nt 2903-3438 and probe 2: nt 4561-5098) were generated by RT-PCR and cloned into the *Bam*HI and *Hin*dIII sites of pBluescript II KS+ vector. Sense or antisense ^{35}S-labeled cRNA probes were generated from these *Pds5B* fragments and in situ hybridization was performed as previously described (Song et al., 2002). Frozen sections (12 μm) were mounted on poly-L-lysine-coated slides, fixed in cold 4% paraformaldehyde in PBS, acetylated and hybridized at 45°C for 4 hours in hybridization buffer containing the ^{35}S-labeled antisense cRNA probes. After hybridization, the sections were treated with RNase A (20 μg/ml) at 37°C for 20 minutes. RNase A-resistant hybrids were detected by autoradiography. Sections hybridized with the sense probes served as negative controls.

Quantitative RT-PCR

RNA was prepared from mouse adult and embryonic tissues using Trizol (Invitrogen) and quantified by the Ribogreen fluorometric assay (Molecular Probes). Reverse transcription was performed using M-MLV reverse transcriptase (Invitrogen) and oligo(dT) and random hexamers as primers. qRT-PCR was performed using a Model 7700 instrument (Applied Biosystems) using *Sybr* Green I fluorescence (Molecular Probes) as described previously (Svaren et al., 2000). Target genes were analyzed using standard curves to determine relative levels of gene expression. Individual RNA samples were normalized according to the levels of GAPDH or 18S mRNA. (See below for primer sequences.)

Primers used for qRT-PCR analysis: mouse *Pds5B*, ACCCTCCTGGAGTCAAGGAAA and CAGAGTCCTGGTCCATGTCCAT; mouse GAPDH, TGCCCCCATGTTTGTGATG and TGTGGTCATGAGCCCTTCC; mouse 18S ribosomal RNA, CGGCTACCACATCCAAGGAA and GCTGGAATTACCGCGGCT.

Plasmids and cell culture

Flag-tagged human *PDS5A* in *pCR3.1* expression vector and the human *PDS5B* (KIAA0979) cDNA were gifts from Kasid Usha (Georgetown University, DC, USA) and Kazusa DNA Research Institute (Chiba, Japan), respectively. To generate the carboxyl-terminal EGFP-PDS5B fusion protein, KIAA0979 was digested with *Bam*HI and *Eco*RI, blunted with Klenow, and cloned into the blunted *Xho*I site in pEGFP-C1 (Clontech). The EGFP-FLAG-PDS5A fusion protein was generated by digesting the *Flag-PDS5A* construct with *Pme*I and inserting this fragment into the blunted *Bgl*II site of pEGFP-C1. HeLa cells were cultured in DMEM with 10% fetal bovine serum. Transient expression of EGFP-tagged PDS5A and PDS5B was achieved using Lipofectamine-mediated transfection of plasmids.

RESULTS

Generation of *Pds5B*-deficient mice

As an initial investigation of PDS5B function we surveyed *Pds5B* mRNA expression levels in adult and embryonic mouse tissues. In the adult we found the highest levels of *Pds5B* expression in brain and testis (Fig. 1A). At the cellular level, in situ hybridization experiments revealed high *Pds5B* expression in neurons of adult hippocampus and dentate gyrus (Fig. 1C). In the testis, high PDS5B expression was detected at the periphery of the seminiferous tubules in a pattern consistent with immature germ cells (Fig. 1B). In the embryo, *Pds5B* expression was comparable in all tissues examined (data not shown), and in situ hybridization revealed that *Pds5B* was ubiquitously expressed at the cellular level (Fig. 1D).

The expression of PDS5B, a regulatory factor of cohesin, in post-mitotic as well as dividing cells, suggested that it participates in multiple processes in mammals. Therefore, to determine its physiological roles in mice, we generated *Pds5B* null mice by homologous recombination (Fig. 1E-G). To confirm the absence of *Pds5B* expression in the homozygous *Pds5B* mice, we quantified *Pds5B* mRNA in E14.5 *Pds5B*$^{-/-}$ brain and examined PDS5B levels in *Pds5B*$^{-/-}$ limbs by western blotting using PDS5B antibodies. We did not detect *Pds5B* mRNA or protein (Fig. 1H,I; see Fig. S1 in the supplementary material) in embryos homozygous for the mutant *Pds5B* allele, indicating that it is a true null allele. *Pds5B*$^{-/-}$ embryos were present at the expected Mendelian ratio until age E16.5. However, only about 75% of the expected number of *Pds5B*$^{-/-}$ fetuses were born alive and none of the mice homozygous for the mutant *Pds5B* allele survived beyond P1. The newborn animals had signs of respiratory distress, including labored breathing, use of accessory muscles of respiration as indicated by head bobbing and intercostal and abdominal retractions, cyanosis and pallor. They all died shortly after birth, most probably from cardiac and/or respiratory abnormalities (see below).

Pds5B deficiency results in growth retardation, abnormal skeletal patterning and cleft palate

Wild-type and *Pds5B*$^{-/-}$ mutant embryos were of similar size until E16.5, but then the mutants began to show signs of growth retardation. Newborn Pds5B$^{-/-}$ mice were smaller than their wild-type littermates, and had short stature, short limbs, a small head and facial dysmorphisms (short snout, short low chin and thin upper lip; Fig. 2A-C,K). These abnormalities, which are similar to those reported for CdLS patients, along with the fact that mutations in other cohesion proteins are associated with CdLS, suggested to us

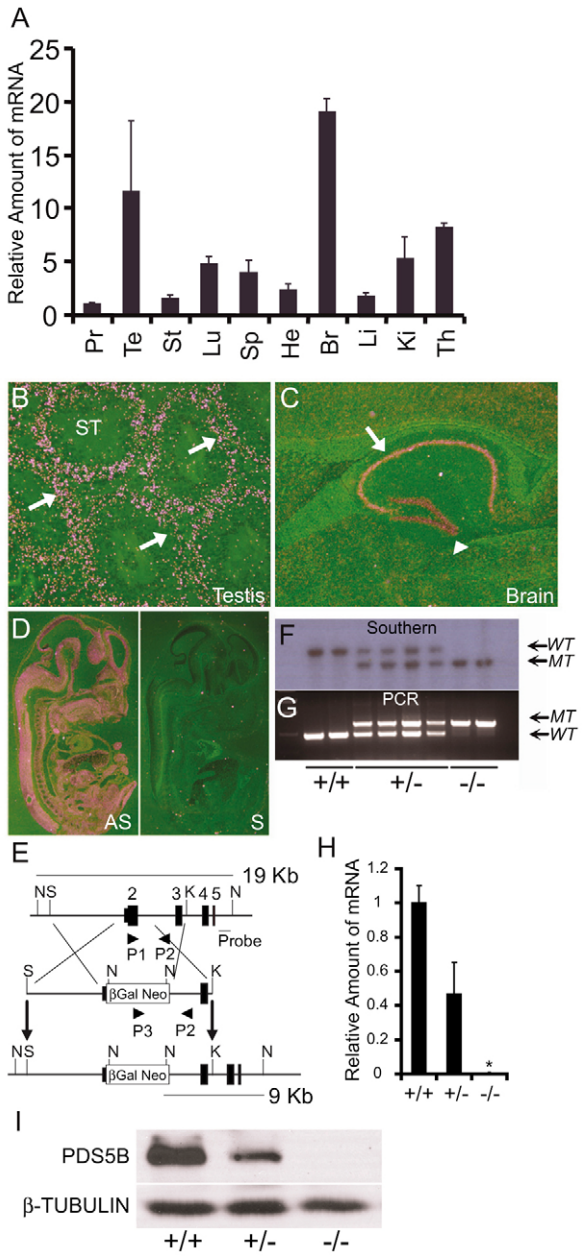

Fig. 1. Expression of *Pds5B* and generation of *Pds5B*-deficient mice. (**A**) Quantitative RT-PCR analysis of *Pds5B* mRNA levels in adult mouse tissues normalized to *18S* RNA. (Pr, prostate; Te, testis, St, stomach; Lu, lung; Sp, spleen; He, heart; Br, brain; Li, liver; Ki, kidney; Th, thymus). Error bars represent ± s.e.m. (**B**,**C**,**D**) Radioactive in situ hybridization (ISH) using ^{35}S-CTP-labeled probes was performed using WT adult testis (B), adult brain (C), and E13.5 embryo (D). Silver grains indicate *Pds5B* mRNA. The green background is the Eosin counterstain visualized by darkfield microscopy. Note the high signal at the periphery of the seminiferous tubules (ST) consistent with *Pds5B* expression in immature germ cells (arrows in B), in hippocampus (arrow in C) and dentate gyrus (arrowhead in C), and wide spread expression in the E13.5 mouse embryo (D). In D, the sagittal sections are probed with antisense (AS, left) and sense control (S, right) probes. (**E**) Schematic representation of homologous recombination between *Pds5B* gene (top) and the targeting construct (middle) to give the mutant *Pds5B* allele (bottom). The coding region of the second exon of *Pds5B* is replaced by a β-gal/*PGK-Neo* (βGal Neo) cassette. The floxed PGK-Neo cassette was later excised by mating to β-actin Cre mice. K, *Kpn*I; N, *Nhe*I; S, *Sac*I. Black bars with numbers indicate exons and P1-P3 indicate positions of primers used for genotyping. (**F**) Southern blot analysis depicting successful targeting of the *Pds5B* locus using genomic DNAs from tails of wild-type (+/+), heterozygous (+/–), homozygous (–/–) mice. The DNA samples were digested with *Nhe*I and hybridized with the radiolabeled DNA probe, indicated in E. (**G**) PCR genotyping analysis of the *Pds5B* mutation was performed with primers P1, P2, and P3 indicated in E. (**H**) Relative amounts of *Pds5B* mRNA from wild-type (+/+), heterozygous (+/–) and homozygous (–/–) embryonic E14.5 brains using qRT-PCR normalized to *GAPDH* mRNA level. Error bars represent the s.e.m. **P*<0.001, Student's unpaired *t*-test. (**I**) Western blot on E14.5 forelimb tissue lysates was probed with antibodies to PDS5B and β-tubulin. Note undetectable PDS5B protein in *Pds5B*$^{-/-}$ lysate.

that the *Pds5B*-deficient mice could be a valuable model of this developmental syndrome. To substantiate this idea, we searched for other abnormalities in *Pds5B*$^{-/-}$ mice that are commonly found in patients with CdLS.

To test for skeletal abnormalities similar to those in CdLS patients, we stained wild-type and mutant embryos with Alizarin Red S and Alcian Blue to highlight the skeleton, and found that several bones including the mandible, ulna, radius, humerus and scapula were shorter in the *Pds5B*$^{-/-}$ mice (Fig. 2D-F). Shortened limbs are associated with mild cases of CdLS (Ireland et al., 1993); however, we did not observe the limb truncations or fused digits (syndactyly) that are observed in more severely affected CdLS patients. All *Pds5B*$^{-/-}$ mice exhibited sternal malformations [wild type (WT): 0/24; *Pds5B*$^{-/-}$: 37/37] characterized by either two unfused ossification centers or lack of ossification of the sternebrae (Fig. 2G). In addition, the sternums of *Pds5B*$^{-/-}$ mice were shorter than those of wild-type mice (Fig. 2G). We also found other abnormalities in skeletal patterning, with incomplete penetrance and variable expressivity, including delayed ossification of digital bones and vertebrae (data not shown), fusion of extensively ossified rib anlage at C7 and the costal cartilage of the T1 rib (WT: 0/10; *Pds5B*$^{-/-}$: 10/18; Fig. 2H), loss or hypoplasia of the 13th ribs (WT: 0/10; *Pds5B*$^{-/-}$: 20/20), and unfused ossification centers in the vertebrae (WT: 0/10; *Pds5B*$^{-/-}$: 5/18; Fig. 2I) and hyoid bone (data not shown).

Another developmental abnormality observed in some children with CdLS is cleft palate. An examination of this region in *Pds5B*$^{-/-}$ mice revealed a complete cleft of the secondary palate (Fig. 2J,K) and failure of the posterior palatal bones to extend fully and meet at the midline (Fig. 2L,M; WT: 0/24; *Pds5B*$^{-/-}$: 25/33). To further characterize the dysmorphogenesis of the palatal shelves in *Pds5B* mutant embryos, we examined the palatal shelves of wild-type and *Pds5B*$^{-/-}$ embryos at E12.5, E14.5 and E18.5. Whereas palatal shelves (PS) in *Pds5B*$^{-/-}$ embryos were seemingly normal at E12.5 (Fig. 2N,Q), by E14.5 they were clearly abnormal (Fig. 2O,R). In E18.5 wild-type embryos, the medial-edge epithelia of the two PS have normally fused and then degenerated (Fig. 2P), however, the PS of E18.5 *Pds5B*$^{-/-}$ embryos were shorter and failed to fuse (Fig. 2S). Using BrdU and TUNEL analysis on E13.5 embryonic palates, we did not observe significant changes in cell proliferation or apoptosis in palatal shelves of *Pds5B*$^{-/-}$ embryos compared to WT or *Pds5B*$^{+/-}$ embryos (see Fig. S2 in the supplementary material).

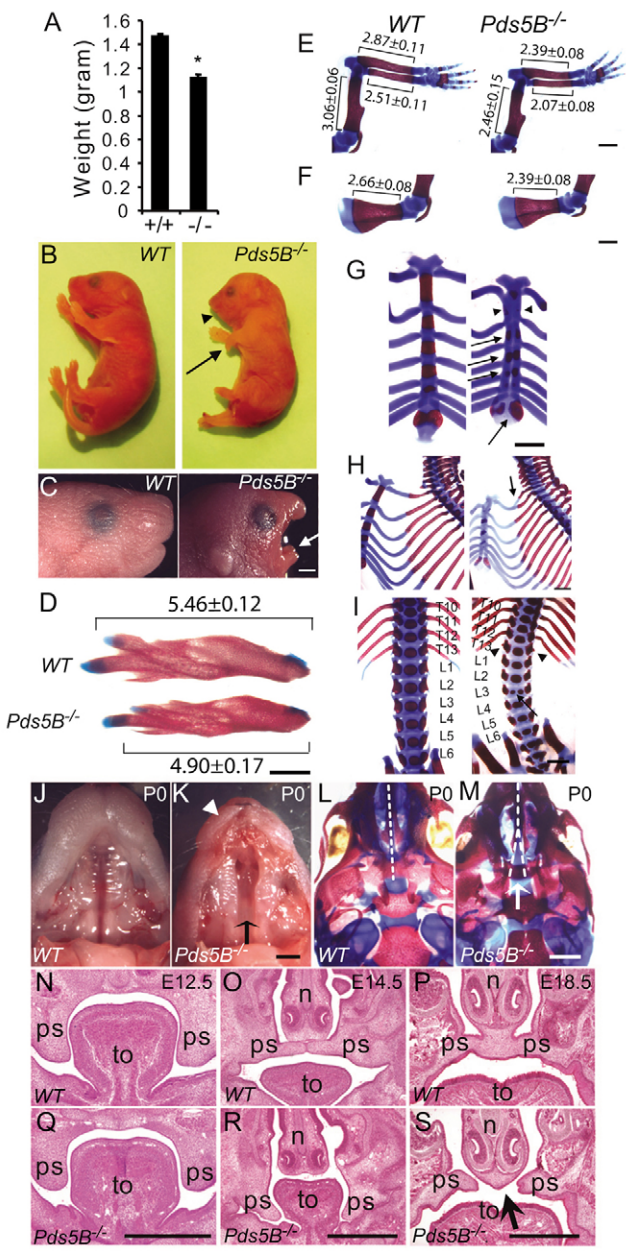

Fig. 2. *Pds5B* deficiency results in growth retardation, abnormal skeletal patterning and cleft palate. (**A**) The weight of *Pds5B*$^{-/-}$ P0 mice is lower than that of wild-type littermates (WT, *n*=43 and *Pds5B*$^{-/-}$ mice, *n*=35). Error bars represent s.e.m. **P*<0.001, Student's unpaired *t*-test. (**B,C**) Morphology of wild-type and mutant mice. (B) Note short stature, facial dysmorphism, short limbs (arrow), short snout (arrowhead), and small head in *Pds5B*$^{-/-}$ compared to wild-type P0 mice. (C) Short mandible (arrow) in *Pds5B*$^{-/-}$ neonate (right) compared to wild-type (left). (**D-I**) Alizarin Red S and Alcian Blue staining of newborn mouse skeleton. Red indicates bone and blue indicates cartilage. (D) Mandibles; (E) ulna, radius and humerus of forelimbs; (F) scapula of forelimbs. Bone lengths (square bracket) are indicated by numbers (lengths in mm ± s.d.). Note the length of mandible, ulna, radius and humerus is significantly shorter in *Pds5B*$^{-/-}$ compared to wild-type. Sample sizes for each genotype range from 18 to 34. *P*<0.001, Student's unpaired *t*-test. (G) Sternum. Arrows, unfused ossification centers; arrowheads, delayed or missing ossification centers. (H) Ribs. The arrow points to the C7-T1 fusion. (I) Thoracic (T) and lumbar (L) vertebrae. The arrow points to the unfused L3 vertebra and arrowheads point to the hypoplastic 13th ribs in *Pds5B*$^{-/-}$ neonate. (**J,K**) Complete cleft palate (arrow) and thin upper-lip (arrowhead) of a *Pds5B*$^{-/-}$ neonate (K) compared with wild-type control (J). (**L,M**) Alizarin Red S and Alcian Blue staining of neonate skulls. The edges of palatal bones are marked by dashed lines. Posterior parts of the palatal bones in *Pds5B*$^{-/-}$ mutant failed to meet at the midline (arrows, M), compared with wild-type littermate (L). (**N-S**) Palatogenesis defects illustrated using H&E stained coronal sections of wild-type and *Pds5B*$^{-/-}$ E12.5, E14.5, and E18.5 embryos. Wild-type (N-P); *Pds5B*$^{-/-}$ (Q-S). ps, palatal shelf; n, nasal bone; to, tongue. Arrow in S points to the unfused palatal shelves. Scale bars:1 mm.

The cleft palate observed in *Pds5B*$^{-/-}$ mice could be the result of abnormal reorientation of palatal shelves or failure of epithelial-mesenchymal transition of medial edge epithelia at a later stage. Clearly, cleft palate is a distinctive feature of *Pds5B*$^{-/-}$ mice and could cause aspiration and subsequent asphyxiation, thus contributing to the neonatal lethality of these mice.

PDS5B is important for cardiac development

Because children with CdLS often have congenital heart defects and *Pds5B*$^{-/-}$ mice suffer respiratory distress and perinatal lethality, we searched for cardiac malformations. The incidence of congenital heart defects of any type was significantly higher in *Pds5B*$^{-/-}$ compared to wild-type mice (15/24 versus 0/14, *P*<0.001; Fig. 3A-G). The defects included those that are commonly found in CdLS patients (Jackson et al., 1993). We identified atrial septal defects of the secundum type (ASD, 6/24), ventricular septal defects (VSD, 12/24; ten perimembranous, one muscular, one inlet), and a common atrioventricular canal defect (1/24; Fig. 3C-F) in these mice. Of note, one *Pds5B*$^{-/-}$ mouse had a large perimembranous VSD with anterior malalignment of the outlet septum, causing the aorta to shift over the VSD toward the right ventricle (Fig. 3C). This mouse did not have right ventricular outflow tract obstruction and thus had the forme fruste of tetralogy of Fallot, a common malformation in CdLS. The VSDs and common AV canal defects would be expected to cause pulmonary overcirculation and edema from left-to-right shunting of blood at the ventricular level, thus resulting in respiratory distress and potentially contributing to early postnatal lethality of *Pds5B*$^{-/-}$ mice.

PDS5B-deficiency causes abnormal peripheral nervous system development

The high expression of *Pds5B* in post-mitotic neurons, the role of other cohesion components such as *Mau-2* in axonal guidance and neuronal migration, and the profound mental retardation associated with CdLS, encouraged us to examine the nervous system in *Pds5B*$^{-/-}$ mice. Consistent with clinical reports showing that CdLS patients have relatively normal brain anatomy, we did not observe any gross or microscopic structural abnormalities in the brain of *Pds5B*-deficient mice. This suggests that the cohesin complex does not play a major role in CNS development; instead, it may influence neuronal function or connectivity. Unfortunately, the neonatal lethality of *Pds5B*$^{-/-}$ mice currently prevents us from further examining this hypothesis.

An examination of the peripheral nervous system revealed that the sympathetic chain ganglia were well developed with neuronal projections appearing normal in *Pds5B*$^{-/-}$ mice (see Fig. S3 in the

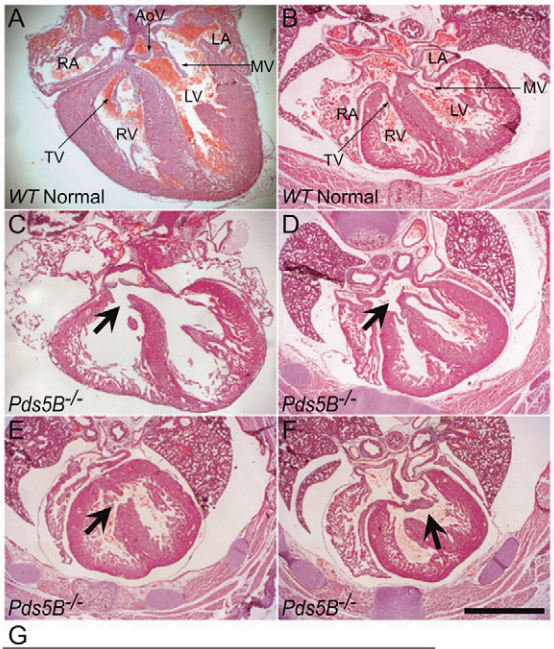

G

	ASD	VSD	CAVC	Total	
WT	0/14	0/14	0/14	0/14	$p < 0.001$
Pds5B$^{-/-}$	6/24	12/24	1/24	15/24	

Fig. 3. Congenital heart defects in *Pds5B*$^{-/-}$ mice mimic those observed in CdLS patients. (**A,B**) Sections of wild-type mouse hearts demonstrating (A) the intact ventricular septum and relationships of the aortic, tricuspid and mitral valves, and (B) an intact atrial septum. (**C-F**) Sections of mutant mouse hearts showing: (C) a large perimembranous VSD with the aorta riding over both ventricles; (D) a secundum ASD; (E) a muscular VSD; (F) a common atrioventricular canal defect. Note the single atrioventricular valve and the common defect of the atrial and ventricular septum. Arrows indicate the respective defects. AoV, TV, MV, aortic, tricuspid and mitral valve; RA, LA, right, left atrium; RV, LV, right, left ventricle. Scale bar: 1 mm. (**G**) Summary of congenital heart defects in *Pds5B*$^{-/-}$ mice. *P*<0.001 is calculated by a Z-test for significant differences in total incidence between WT and *Pds5B* homozygotes.

supplementary material). We also examined the superior cervical ganglia (SCG), which provides sympathetic innervation to the ocular muscles. Abnormalities in the SCG are associated with ptosis, a common condition in CdLS. We found a number of abnormalities in the SCG and its projections to target organs in the *Pds5B*$^{-/-}$ mice (Fig. 4A). For example, in 40% (5/13) of *Pds5B*$^{-/-}$ mice, the SCG was located far caudal of its normal position (Fig. 4B,C). Furthermore, all *Pds5B*$^{-/-}$ mice had thin carotid nerves (Fig. 4D,E) and 30% (4/13) of these mice had unilateral or bilateral absence of the carotid nerve (Fig. 4F,G). These SCG defects are similar to those observed in mice deficient for the neurotrophic factor artemin, which commonly manifest unilateral or bilateral ptosis (Honma et al., 2002). These results suggest that SCG innervation defects are the likely cause of the ptosis observed in many CdLS patients (Jackson et al., 1993).

We next examined the enteric nervous system (ENS), a complex network of neurons and glia within the bowel that is derived from migrating neural crest cells (NCCs). The NCCs migrate in a proximal to distal direction along the length of the bowel and normally reach the mid-colon by E12.5 (Fig. 4H). By contrast, in *Pds5B*$^{-/-}$ mice, ENS precursors failed to migrate past the ileocecal (IC) junction by this age (Fig. 4I). Furthermore, even in regions of the distal bowel colonized by NCCs, the neuronal density was lower in *Pds5B*$^{-/-}$ mice compared to wild-type animals (data not shown).

To determine if the enteric neuron defects occur because of delayed migration of NCCs into the colon, we examined the ENS at E18.5 and P0 using the Tuj1 antibody, which recognizes a neuronal form of tubulin, or acetylcholinesterase (AchE) staining (Fig. 4J-M; see Fig. S3 in the supplementary material). As expected, enteric neurons colonize the entire length of the wild-type neonatal bowel (Fig. 4J,L), whereas 70% (8/12) of *Pds5B*$^{-/-}$ mice exhibited variable degrees of abnormal innervation and ganglion formation in the distal colon (Fig. 4K,M). By contrast, small bowel innervation appeared grossly normal in *Pds5B*$^{-/-}$ mice (data not shown). Thus, the majority of *Pds5B*$^{-/-}$ mice had significant defects in the distal enteric nervous system that resemble Hirschsprung disease in humans. This contrasts with CdLS where distal colonic aganglionosis has not been reported, but where other gastrointestinal problems including persistent emesis and feeding problems are common, occurring in 62% and 77%, respectively, of infants with CdLS (Jackson et al., 1993). These observations suggest that defects in the ENS such as hypoganglionosis may underlie the gastrointestinal symptoms of CdLS patients.

PDS5B regulates primordial germ cell proliferation

The high expression of *Pds5B* in adult and embryonic testis, the role of PDS5 in mitosis and meiosis in lower organisms, and the high frequency of genital anomalies seen in people with CdLS, encouraged us to examine germ cell development in *Pds5B*$^{-/-}$ mice. We found a severely reduced number of germ cells in testes and ovaries of newborn *Pds5B*$^{-/-}$ mice (Fig. 5A-D; see Fig. S4 in the supplementary material) that appeared to be more severe in males. We therefore focused on male germ cell development to further investigate mechanisms underlying germ cell depletion. At E16.5, *Pds5B*$^{-/-}$ male mice had an 80% reduction in germ cells in the testis (Fig. 5E,F,I). To determine if the remaining germ cells could undergo spermatogenesis, we performed testis transplantation to propagate E16.5 testis of wild-type and *Pds5B*$^{-/-}$ mice as explants in nude mice (Naughton et al., 2006). Using GCNA1 immunohistochemistry, we found a complete depletion of spermatogonial stem cells at 2 weeks after transplantation (Fig. 5G,H). By 6 weeks after transplantation, the explanted *Pds5B*$^{-/-}$ testes contained testicular cords that only contained Sertoli cells (see Fig. S4 in the supplementary material). The *Pds5B*$^{-/-}$ Sertoli cells were morphologically normal as determined by GATA4 immunohistochemistry (data not shown). These studies indicate that the germ cells remaining at E16.5 in *Pds5B*$^{-/-}$ mice were incapable of sustaining spermatogenesis.

The embryonic loss of germ cells at E16.5 in *Pds5B*-deficient mice suggested that PDS5B is important for primordial germ cell (PGC) development. PGCs are derived from a founder population of ~45 cells in the extraembryonic mesoderm posterior to the primitive streak around E7.25 (Ginsburg et al., 1990). These cells migrate to the genital ridge by E11.5 (Gomperts et al., 1994), and continue proliferating until E13.5 in males (McLaren, 2000). To identify the mechanism underlying the reduced number of germ cells in male *Pds5B*$^{-/-}$ mice, we evaluated the migration, proliferation and apoptosis of these germ cell precursors. At E12.5, a time point when PGCs enter the genital ridge, there were already significantly fewer numbers of germ cells in the *Pds5B*$^{-/-}$ mice. We hypothesized that overt migration defects in

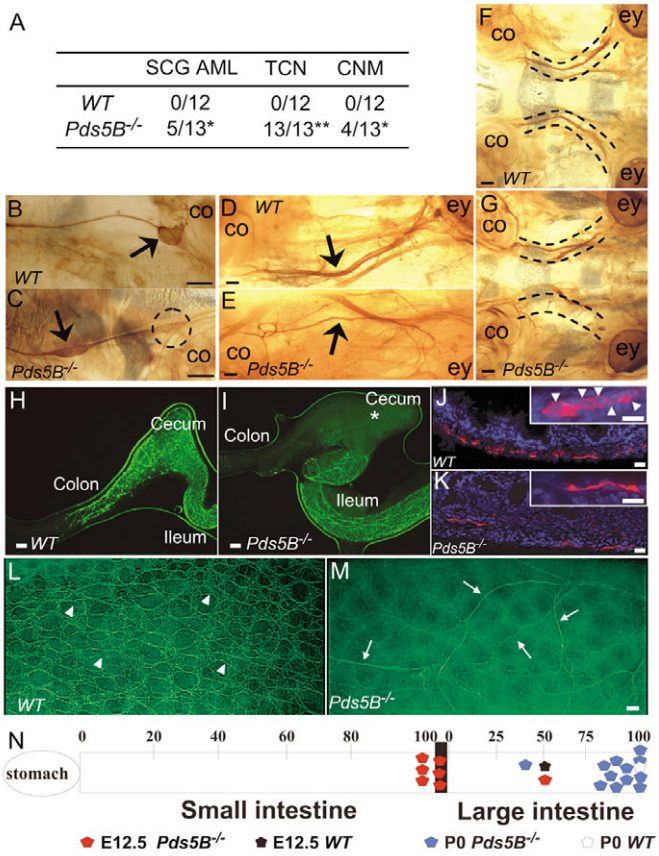

Fig. 4. *Pds5B*$^{-/-}$ mice display multiple defects in the peripheral nervous system. (**A**) Summary of carotid nerve and superior cervical ganglion (SCG) abnormalities in *Pds5B*-deficient mice. SCG AML, SCG delayed migration or abnormal localization; TCN, thin carotid nerve; CNM, carotid nerve missing. **P*<0.05 and ***P*<0.001 determined by a Z-test for significant differences in incidence between WT and *Pds5B* homozygotes. (**B-G**) TOH whole-mount staining of sympathetic neurons of neonate mice. (B,C) Abnormal caudal location of SCG in *Pds5B*$^{-/-}$ mice compared to wild-type mice (SCG, arrows). Dashed circle indicates the expected normal location of SCG (C). Note the severe reduction or absence of carotid nerves in *Pds5B*$^{-/-}$ (E,G) compared to WT mice (D,F). Carotid nerves are indicated by arrows in D and E, and by two dashed lines in F and G. ey, eye; co, cochlea. Scale bars: 400 μm (B-E); 200 μm (F,G). (**H**,**I**) E12.5 enteric neurons in the distal bowel of whole gut demonstrated by TuJ1 immunohistochemistry (H, wild type; I, *Pds5B*$^{-/-}$). *, ileocecal junction. Note that the enteric neuron migration wave front did not pass the ileocecal junction in *Pds5B*$^{-/-}$ mice (I). Scale bars: 10 μm (H,I). (**J**,**K**) TuJ1 staining of P0 paraffin sections of distal colon from wild-type (J) and *Pds5B*$^{-/-}$ mice (K), showing the lack of clustered enteric neuron cell bodies in *Pds5B*$^{-/-}$ mice. Scale bars: 20 μm. (Insets) High magnification of TuJ1 staining of P0 distal colons. Scale bars: 10 μm. Arrowheads point to the clustered enteric neuron cell bodies. (**L**,**M**) Tuj1 whole-mount staining of E18.5 guts from wild-type mice (L) and *Pds5B*$^{-/-}$ (M). Wild-type mice show normal formation of enteric plexus with clustered neuronal cell bodies (arrowheads) in the mid-colon, whereas *Pds5B*$^{-/-}$ mice lack enteric neuron cell bodies and show only a few thin nerve fibers (arrows). Scale bar: 100 μm. (**N**) Schematic representation of ENS defects in *Pds5B*$^{-/-}$ mice [E12.5: *Pds5B*$^{-/-}$ (*n*=7) and WT (*n*=9); P0: *Pds5B*$^{-/-}$ (*n*=12) and WT (*n*=13)]. The scale at the top corresponds to the percentage of the respective intestinal segment (small or large intestine) successfully colonized by neurons.

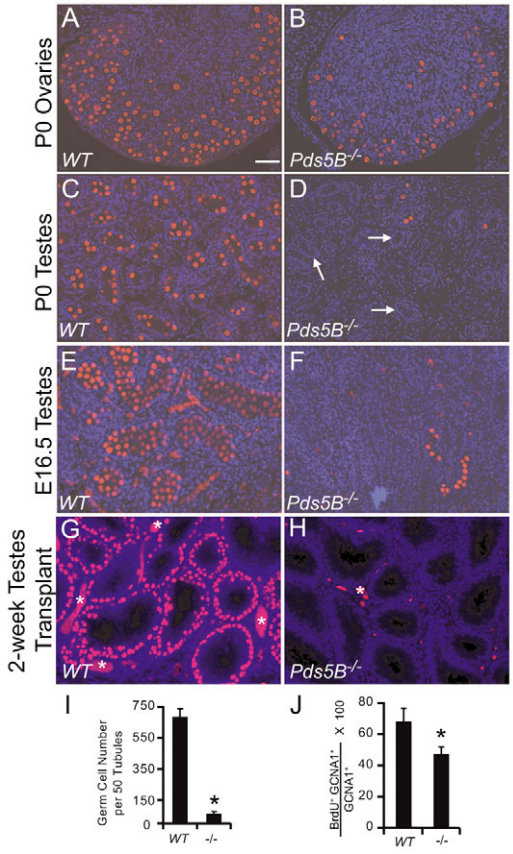

Fig. 5. *Pds5B*-deficient mice manifest germ cell defects. GCNA1 staining of germ cells of WT (**A**) and *Pds5B*$^{-/-}$ (**B**) neonatal ovaries, and WT (**C**) and *Pds5B*$^{-/-}$ (**D**) neonatal testes show reduced germ cells in *Pds5B*$^{-/-}$ mice. Arrows point to empty testicular cords in D. (**E**,**F**) GCNA1 immunohistochemical analysis of E16.5 germ cells in WT (E) and *Pds5B*-deficient (F) testes shows a reduction in germ cells during embryogenesis. (**G**,**H**) GCNA1 staining of two-week testes transplants of E16.5 wild-type (G) and *Pds5B*$^{-/-}$ mice (H). In contrast to the presence of germ cells in the periphery of WT seminiferous tubules (G), note complete loss of germ cells in *Pds5B*$^{-/-}$ testis explant (H). *Non-specific auto-fluorescence signal; red, GCNA1; blue, bisbenzimide. (**I**) Quantitative analysis of germ cells in E16.5 testes of WT and *Pds5B*-deficient mice (*n*=4 for each genotype). Error bars represent SEM. **P*<0.001, Student's unpaired *t*-test. (**J**) Proliferation index measured by BrdU incorporation in GCNA1-positive germ cells at E12.5 (*n*=3 for each genotype and 100 GCNA1-positive cells were counted for each animal). Error bars represent s.e.m. **P*<0.05, Student's paired *t*-test. Scale bars: 50 μm.

Pds5B$^{-/-}$ PGCs would result in failure of these precursors to reach the genital ridge by E11.5. However, alkaline phosphatase staining of E10.5 gonads to identify PGCs revealed no significant differences in PGC location between wild-type and *Pds5B*$^{-/-}$ embryos (data not shown), indicating that PGC migration at this early stage must be relatively normal. In addition, TUNEL analysis revealed no changes in the number of apoptotic germ cells in E12.5 or E16.5 mutant embryos (data not shown). However, when we examined germ cell proliferation in E12.5 embryos using BrdU incorporation, we found a 30% reduction in the number of BrdU-positive germ cells in testes of *Pds5B*$^{-/-}$ versus wild-type mice (Fig. 5J; see Fig. S4 in the supplementary material). Although it is possible that germ cell depletion could be partially due to apoptosis or delayed migration at stages in development that we did not examine, it is clear that the reduced proliferation is a major factor in the reduced number of germ cells.

PDS5B loss does not alter sister chromatid cohesion

PDS5 is crucial for sister chromatid cohesion (Dorsett et al., 2005; Hartman et al., 2000; Losada et al., 2005; Panizza et al., 2000; van Heemst et al., 1999; Wang et al., 2003; Wang et al., 2002). To test for cohesion defects in *Pds5B*-deficient mammalian cells, we performed GTW metaphase chromosome banding of mouse embryonic fibroblast (MEF) chromosomes. Two MEF lines were obtained from both *Pds5B*-deficent and wild-type mice. Quantitative RT-PCR and western blot analyses were performed and we found that these cells were indeed devoid of both *Pds5B* mRNA and protein (see Fig. S1 in the supplementary material). We analyzed a total of 22-25 metaphase cells per line (two WT and two *Pds5B*$^{-/-}$ MEF lines; detailed results are available on request). No obvious cohesion defects such as precocious sister chromatid separation (PSCS) or gross chromosomal abnormalities were observed in the *Pds5B*$^{-/-}$ MEFs (Fig. 6A,B). The lack of sister chromatid cohesion abnormalities in *Pds5B*-deficient cells suggests that PDS5B has novel functions other than sister chromatid cohesion that are important for mammalian embryonic development.

The wide ranging deficits in the *Pds5B*$^{-/-}$ mice suggested that PDS5B has acquired additional functional domains during evolution. To examine this possibility, we performed motif searching of mouse PDS5B using Blocks and Pfam motif libraries with the default cut-off scores. We identified the previously reported HEAT repeats within the N terminus (Losada et al., 2005; Neuwald and Hirano, 2000; Panizza et al., 2000) and two AT hook domains in the C terminus that closely match the high mobility group protein (HMGY) signature (Block IPB000116A). Further analysis revealed that these AT hook domains are present in PDS5B from fish to human (Fig. 6C), but are not present in the yeast, worm and fly orthologs. The AT hook domain was initially identified in the HMG-I/Y family as a domain that binds to AT tracts in the minor groove of DNA (Maher and Nathans, 1996). The identification of AT hook domains in PDS5B is the first recognizable DNA binding motif reported in a sister chromatid cohesion factor, indicating that PDS5B and the cohesin complex may regulate gene transcription through direct cohesin complex-DNA interactions mediated by PDS5B.

There are two PDS5 homologs in vertebrates (Losada et al., 2005). The N-terminal regions of these proteins both contain HEAT repeats and are closely related, but PDS5A lacks the AT hook domains present in the C-terminal region of PDS5B. Despite their similarity, the severe abnormalities caused by PDS5B deficiency clearly show that PDS5A cannot compensate for at least some of the physiologic roles of PDS5B. We investigated whether their distinct cellular functions could stem, at least in part, from differential subcellular localization of these two proteins. We generated EGFP-tagged PDS5A and PDS5B fusion proteins and determined their subcellular localization in interphase cells using fluorescence microscopy. Whereas both PDS5A and PDS5B were found in the nucleus, PDS5B appeared to be more concentrated in the nucleolus than in the rest of the nucleus. By contrast, PDS5A was less abundant in the nucleolus than in the rest of the nucleus (Fig. 6D).

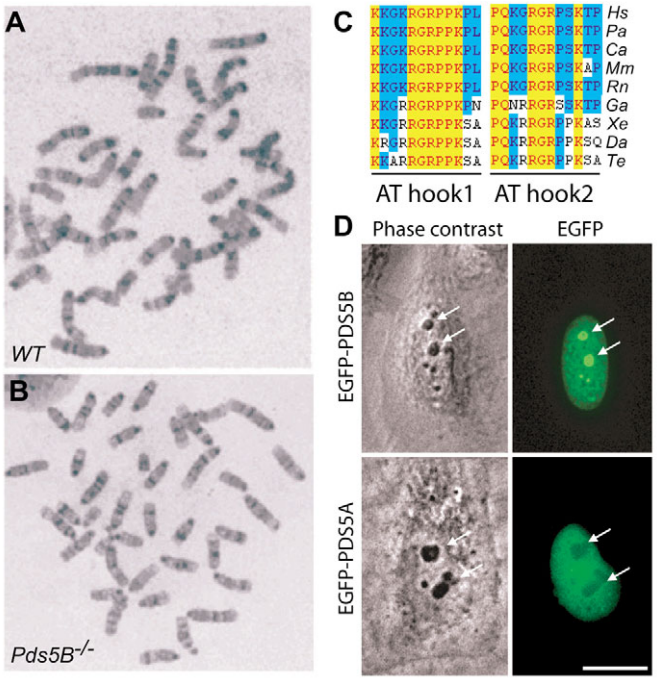

Fig. 6. *Pds5B*$^{-/-}$ MEFs lack sister chromatid cohesion defects. (**A**,**B**) Metaphases from mouse embryonic fibroblasts (MEFs) derived from WT and *Pds5B*$^{-/-}$ mice show no differences in sister chromatid cohesion. (**C**) Multi-species alignment of AT hook domains of PDS5B. *Hs, Homo sapiens; Pa, Pan troglodytes; Ca, Canis familiaris; Mm, Mus musculus; Rn, Rattus norvegicus; Ga, Gallus gallus; Xe, Xenopus tropicalis; Da, Danio rerio; Te, Tetraodon nigroviridis*. (**D**) Subcellular localization of human homologs of PDS5 using EGFP-tagged PDS5A and PDS5B fusion proteins. HeLa cells were transfected with EGFP-PDS5A and EGFP-PDS5B using Lipofectamine. At 24 hours later, the EGFP signals were examined. Left panels are phase-contrast images of HeLa cells; right panels are images of GFP signals. Note that EGFP-PDS5B is present in the nucleus and highly enriched in the nucleolus (arrows), whereas EGFP-PDS5A is localized to the nucleus but excluded from the nucleolus (arrows). Scale bar: 5 μm.

DISCUSSION

Mutations in four different cohesion proteins (NIPBL, SMC1A, SMC3 and ESCO2) have been found in patients with CdLS and Roberts syndrome/SC phocomelia (RBS/SC), and are thought to be responsible for the broad spectrum of prenatal and postnatal developmental anomalies (Deardorff et al., 2007; Krantz et al., 2004; Musio et al., 2006; Schule et al., 2005; Tonkin et al., 2004; Vega et al., 2005). These observations clearly indicate that sister chromatid cohesion factors are important for early development of multicellular organisms, either through abnormalities in chromosome dynamics or via alternative functions.

In this work, we generated mice deficient in *Pds5B*, a sister chromatid cohesion factor. These mice manifest a spectrum of developmental defects similar to those found in human CdLS, including abnormal skeletal patterning, cardiac anomalies and cleft palate. Other phenotypes that are associated with CdLS such as mental retardation, hearing loss and gastroesophageal reflex are difficult to evaluate in this animal model particularly since *Pds5B*$^{-/-}$ mice are not viable past P0. However, the striking defects in the enteric and autonomic nervous systems of these mice may be related to the frequent occurrence of ptosis and gastrointestinal problems in CdLS patients. Because of significant phenotypic overlap in *Pds5B*$^{-/-}$ mice and people with CdLS (Table 1), and the fact that mutations in other cohesion factors have been identified in CdLS patients, we believe that *Pds5B*$^{-/-}$ mice represent the first mouse model resembling human Cornelia de Lange syndrome. In fact, the broad spectrum of symptoms with incomplete penetrance and variable expressivity in these mice is also a feature typically

observed in CdLS. These studies and the previously known association of mutations in other cohesion factors and CdLS suggest that screening CdLS patients for *PDS5B* mutations is warranted. *PDS5B* mutations, unless they produce dominant negative mutants, may be rare because they would be recessive and most CdLS cases are dominantly inherited (Krantz et al., 2004; Tonkin et al., 2004), and because they may result in lethality unless they are hypomorphic.

Although the molecular function of PDS5 is still under investigation, several organisms require diverse function of PDS5 for chromatid cohesion (Losada et al., 2005). For example, it may act as a regulator of the SMC ATPase through the HEAT motifs shared by SCC2 (Kimura and Hirano, 2000) and thereby modulate the dynamics of the cohesin ring. Alternatively, PDS5 may act as a scaffolding protein and promote protein-protein interactions between adjacent cohesin complexes (Losada et al., 2005). An examination of the chromosomes from *Pds5B*-deficient mouse cells did not show any abnormalities in sister chromatid cohesion (i.e. PSCS). This result was in contrast to those obtained in budding yeast, worm and *Drosophila*, where PDS5 plays an important role in chromosome segregation (Dorsett et al., 2005; Hartman et al., 2000; Wang et al., 2003). It is possible that our assay in which a total of 50 cells were examined may not have detected subtle defects. Indeed, only mild cohesion defects were found in HeLa cells in which *PDS5B* was knocked down by RNAi (Losada et al., 2005). Furthermore, our results are consistent with reports of the lack of sister chromatid cohesion defects in cells from CdLS patients (Tonkin et al., 2004; Vrouwe et al., 2007) or only mild cohesion defects in 40% of CdLS patients (Kaur et al., 2005). Overall, these results are consistent with our hypothesis that the abnormalities present in patients with CdLS and related diseases probably result from abnormal cohesin-mediated functions other than sister chromatid cohesion (Dorsett, 2007; Krantz et al., 2004; Tonkin et al., 2004). In this regard, it has been hypothesized that the cohesin complex directly binds to regulatory cis-elements and transcriptionally regulates developmental gene expression (Krantz et al., 2004; Rollins et al., 1999; Tonkin et al., 2004). Support for this idea comes from a number of studies in lower organisms. For example, severe cohesion defects have been observed in *Drosophila Pds5* homozygous mutants, but not in heterozygotes, where only defects in *cut* gene expression and wing (limb) development are observed (Dorsett et al., 2005). In this regard, direct interactions of the cohesin complex with multiple sites between the wing margin enhancer and promoter lead to transcriptional regulation of the developmental gene *cut* (Dorsett et al., 2005). Yet another example of alternative Pds5B function is found in yeast *Pds5* mutants, in which topoisomerase II can rescue the lethality, but not the cohesion defect of these mutants (Aguilar et al., 2005). Furthermore, the cohesion protein, MAU-2, is highly expressed in the mammalian adult nervous system and is crucial for neuronal migration and axonal guidance (Seitan et al., 2006; Watrin et al., 2006). PDS5B is also expressed at high levels in neurons, yet its function in adult neurons is unlikely to be related to sister chromatid cohesion as these cells are post-mitotic and thus do not undergo cell division. How cohesin complexes could directly regulate transcription has remained elusive because no DNA binding motifs have been identified in proteins that comprise the cohesin complex or its regulatory factors. Our analysis of PDS5B has identified two AT hook domains, the motif that constitutes the DNA binding domain of HMG proteins (Maher and Nathans, 1996). We propose that PDS5B may constitute an important link in cohesin regulation of transcription through its ability to bind AT rich regulatory sequences and bring the cohesin complex in proximity to promoter elements to regulate transcription.

Table 1. Comparison of clinical and phenotypic features between Cornelia de Lange syndrome and in *Pds5B*$^{-/-}$ mice

	CdLS[a] (%)	*Pds5B*$^{-/-}$ mice (%)
Growth retardation	~100	100
Mental retardation	+	ND
Microcephaly (small head)	93	100
Ptosis	+	100[b]
Thin upper lip	+	+
Micrognathia	84	+
Cleft palate	+	75
Micromelia (small hands and feet)	93	100
Limb-reduction defects/oligodactyly	27	+
Genital hypoplasia (arrested development)	57	100[c]
Gastrointestinal abnormalities	+	70[d]
Hearing loss	60	ND
Heart defects	14	60
Sister chromatid cohesion defects	–[e]	–

The frequency of the feature is indicated by numbers; otherwise, '+' indicates the feature has been reported or observed multiple times and '–' indicates that the feature has not been reported or observed. [a]Data from Jackson et al. (Jackson et al., 1993); [b]Superior cervical ganglion defects that can result in ptosis; [c]Germ cell depletion; [d]Enteric nervous system defects; [e]Data from Tonkin et al. (Tonkin et al., 2004); ND, not determined; CdLS, Cornelia de Lange syndrome.

An alternative explanation for the absence of sister chromatid cohesion defects in *Pds5B*$^{-/-}$ mice could be redundancy with its homolog PDS5A (Losada et al., 2005). Physiological evidence for this will require generation of *Pds5A*$^{-/-}$ animals, but our preliminary studies indicate significant overlap in PDS5A and PDS5B mRNA expression (B.Z. and J.M. unpublished observations). Indeed, we found overlapping expression in a number of organ systems where *Pds5B*$^{-/-}$ mice manifest developmental defects, suggesting differential sensitivity to PDS5B loss in various organs or perhaps reflecting differences in subcellular localization (and function) of these two closely related proteins.

Both PDS5A and PDS5B have previously been reported to be localized in the nucleus by immunohistochemistry (Kumar et al., 2004; Maffini et al., 2002). In these studies, we found that PDS5B is localized to the nucleus with higher levels in the nucleolus. Interestingly, PDS5B lacking the C-terminal 142 residues containing the second AT hook motif was localized to the nucleus but was not concentrated in the nucleolus (B.Z. and J.M., unpublished observation), suggesting that this domain may contribute to its nucleolar localization. Nucleolar localization of PDS5B indicates that PDS5B and/or cohesin complexes containing PDS5B could regulate rRNA metabolism and ribosome biogenesis. Interestingly, other cohesion proteins (e.g. NIPBL and SMC1A) have also been detected in nucleoli (Andersen et al., 2005), and yeast *PDS5* can interact with *NIP7* and *NOP7*, both of which are involved in ribosomal RNA (rRNA) biosynthesis (Davierwala et al., 2005; Krogan et al., 2006). Further evidence of cohesion protein involvement in ribosomal biogenesis comes from studies in yeast, where an additional copy of *NOG2,* which encodes a GTPase required for 60S ribosomal subunit maturation, is able to suppress the defects caused by mutation of the cohesin protein Scc3 (Bialkowska and Kurlandzka, 2002). In addition, the cohesin complex is recruited by Sir2 to silenced chromatin in the rDNA loci to maintain rDNA repeat copy number (Kobayashi et al., 2004). Finally, normal development can be disrupted by defects in rRNA

metabolism, a process largely confined to the nucleolus. For example, *Tcof1*, which encodes a nucleolar protein, is mutated in Treacher Collins syndrome, an autosomal dominant disorder of craniofacial development (Dixon et al., 2006). Haploinsufficiency of *Tcof1* in mice causes a reduction of mature ribosomes that results in deficient neural crest cell migration and proliferation that leads to craniofacial abnormalities, including cleft palate and mandibular hypoplasia (Dixon et al., 2006). Deficits in the nucleolar functions of cohesion proteins could also contribute to the abnormalities observed in patients with CdLS or related diseases.

In summary, we have discovered that the cohesion protein PDS5B is a critical regulator of multiple aspects of organogenesis, probably via roles unrelated to its ancient function in sister chromatid cohesion. This *Pds5B*-deficient mouse provides the first mammalian model to study the molecular mechanisms of developmental functions of the cohesin complex and the pathogenesis of CdLS and related disorders with mutations in cohesion factors.

We are deeply indebted to Robert H. Baloh and Jason A. Gustin for careful review of the manuscript and/or helpful discussions of the data. We thank Kelli Simburger, Shelly Audrain, Amber Nielson, Jack Shields, Jennifer Armon, Amy Strickland, Amanda Knoten, Tatiana Gorodinsky and Nina Panchenko for technical assistance. We are grateful to George C. Enders for GCNA1 antibody, Kasid Usha for *PDS5A* plasmid, Kazusa DNA Research Institute for KIAA0979 cDNA, and Mark Johnston for *pRS315* plasmid and help with yeast gap repair. We thank Chih-Lin Hsieh for providing the chromosomal analysis. This work was supported by NIH grants CA111966, AG13730 and NS039358 (to J.M.), HD047396 (to S.J.), DK57038 and DK6459201 (to R.O.H.), O'BRIEN center for Kidney Disease Research (P30DK079333), and Washington University Cancer Biology Pathway Fellowship (to B.Z.). P.J. is a Scholar of the Child Health Research Center of Excellence in Developmental Biology at Washington University School of Medicine (HD001487).

Supplementary material

Supplementary material for this article is available at http://dev.biologists.org/cgi/content/full/134/17/3191/DC1

References

Aguilar, C., Davidson, C., Dix, M., Stead, K., Zheng, K., Hartman, T. and Guacci, V. (2005). Topoisomerase II suppresses the temperature sensitivity of Saccharomyces cerevisiae pds5 mutants, but not the defect in sister chromatid cohesion. *Cell Cycle* **4**, 1294-1304.

Andersen, J. S., Lam, Y. W., Leung, A. K., Ong, S. E., Lyon, C. E., Lamond, A. I. and Mann, M. (2005). Nucleolar proteome dynamics. *Nature* **433**, 77-83.

Benard, C. Y., Kebir, H., Takagi, S. and Hekimi, S. (2004). mau-2 acts cell-autonomously to guide axonal migrations in Caenorhabditis elegans. *Development* **131**, 5947-5958.

Bialkowska, A. and Kurlandzka, A. (2002). Additional copies of the NOG2 and IST2 genes suppress the deficiency of cohesin Irr1p/Scc3p in Saccharomyces cerevisiae. *Acta Biochim. Pol.* **49**, 421-425.

Davierwala, A. P., Haynes, J., Li, Z., Brost, R. L., Robinson, M. D., Yu, L., Mnaimneh, S., Ding, H., Zhu, H., Chen, Y. et al. (2005). The synthetic genetic interaction spectrum of essential genes. *Nat. Genet.* **37**, 1147-1152.

Deardorff, M. A., Kaur, M., Yaeger, D., Rampuria, A., Korolev, S., Pie, J., Gil-Rodriguez, C., Arnedo, M., Loeys, B., Kline, A. D. et al. (2007). Mutations in cohesin complex members SMC3 and SMC1A cause a mild variant of cornelia de Lange syndrome with predominant mental retardation. *Am. J. Hum. Genet.* **80**, 485-494.

Dixon, J., Jones, N. C., Sandell, L. L., Jayasinghe, S. M., Crane, J., Rey, J. P., Dixon, M. J. and Trainor, P. A. (2006). Tcof1/Treacle is required for neural crest cell formation and proliferation deficiencies that cause craniofacial abnormalities. *Proc. Natl. Acad. Sci. USA* **103**, 13403-13408.

Dorsett, D. (2007). Roles of the sister chromatid cohesion apparatus in gene expression, development, and human syndromes. *Chromosoma* **116**, 1-13.

Dorsett, D., Eissenberg, J. C., Misulovin, Z., Martens, A., Redding, B. and McKim, K. (2005). Effects of sister chromatid cohesion proteins on cut gene expression during wing development in Drosophila. *Development* **132**, 4743-4753.

Enomoto, H., Crawford, P. A., Gorodinsky, A., Heuckeroth, R. O., Johnson, E. M., Jr and Milbrandt, J. (2001). RET signaling is essential for migration, axonal growth and axon guidance of developing sympathetic neurons. *Development* **128**, 3963-3974.

Fu, M., Vohra, B. P., Wind, D. and Heuckeroth, R. O. (2006). BMP signaling regulates murine enteric nervous system precursor migration, neurite fasciculation, and patterning via altered Ncam1 polysialic acid addition. *Dev. Biol.* **299**, 137-150.

Geck, P., Maffini, M. V., Szelei, J., Sonnenschein, C. and Soto, A. M. (2000). Androgen-induced proliferative quiescence in prostate cancer cells: the role of AS3 as its mediator. *Proc. Natl. Acad. Sci. USA* **97**, 10185-10190.

Ginsburg, M., Snow, M. H. and McLaren, A. (1990). Primordial germ cells in the mouse embryo during gastrulation. *Development* **110**, 521-528.

Gomperts, M., Garcia-Castro, M., Wylie, C. and Heasman, J. (1994). Interactions between primordial germ cells play a role in their migration in mouse embryos. *Development* **120**, 135-141.

Hartman, T., Stead, K., Koshland, D. and Guacci, V. (2000). Pds5p is an essential chromosomal protein required for both sister chromatid cohesion and condensation in Saccharomyces cerevisiae. *J. Cell Biol.* **151**, 613-626.

Honaramooz, A., Snedaker, A., Boiani, M., Scholer, H., Dobrinski, I. and Schlatt, S. (2002). Sperm from neonatal mammalian testes grafted in mice. *Nature* **418**, 778-781.

Honma, Y., Araki, T., Gianino, S., Bruce, A., Heuckeroth, R., Johnson, E. and Milbrandt, J. (2002). Artemin is a vascular-derived neurotropic factor for developing sympathetic neurons. *Neuron* **35**, 267-282.

Ireland, M., Donnai, D. and Burn, J. (1993). Brachmann-de Lange syndrome. Delineation of the clinical phenotype. *Am. J. Med. Genet.* **47**, 959-964.

Jackson, L., Kline, A. D., Barr, M. A. and Koch, S. (1993). de Lange syndrome: a clinical review of 310 individuals. *Am. J. Med. Genet.* **47**, 940-946.

Jain, S., Naughton, C. K., Yang, M., Strickland, A., Vij, K., Encinas, M., Golden, J., Gupta, A., Heuckeroth, R., Johnson, E. M., Jr et al. (2004). Mice expressing a dominant-negative Ret mutation phenocopy human Hirschsprung disease and delineate a direct role of Ret in spermatogenesis. *Development* **131**, 5503-5513.

Kaur, M., DeScipio, C., McCallum, J., Yaeger, D., Devoto, M., Jackson, L. G., Spinner, N. B. and Krantz, I. D. (2005). Precocious sister chromatid separation (PSCS) in Cornelia de Lange syndrome. *Am. J. Med. Genet. A* **138**, 27-31.

Kimura, K. and Hirano, T. (2000). Dual roles of the 11S regulatory subcomplex in condensin functions. *Proc. Natl. Acad. Sci. USA* **97**, 11972-11977.

Kobayashi, T., Horiuchi, T., Tongaonkar, P., Vu, L. and Nomura, M. (2004). SIR2 regulates recombination between different rDNA repeats, but not recombination within individual rRNA genes in yeast. *Cell* **117**, 441-453.

Krantz, I. D., McCallum, J., DeScipio, C., Kaur, M., Gillis, L. A., Yaeger, D., Jukofsky, L., Wasserman, N., Bottani, A., Morris, C. A. et al. (2004). Cornelia de Lange syndrome is caused by mutations in NIPBL, the human homolog of Drosophila melanogaster Nipped-B. *Nat. Genet.* **36**, 631-635.

Krogan, N. J., Cagney, G., Yu, H., Zhong, G., Guo, X., Ignatchenko, A., Li, J., Pu, S., Datta, N., Tikuisis, A. P. et al. (2006). Global landscape of protein complexes in the yeast Saccharomyces cerevisiae. *Nature* **440**, 637-643.

Kumar, D., Sakabe, I., Patel, S., Zhang, Y., Ahmad, I., Gehan, E. A., Whiteside, T. L. and Kasid, U. (2004). SCC-112, a novel cell cycle-regulated molecule, exhibits reduced expression in human renal carcinomas. *Gene* **328**, 187-196.

Le, N., Nagarajan, R., Wang, J. Y., Araki, T., Schmidt, R. E. and Milbrandt, J. (2005). Analysis of congenital hypomyelinating Egr2Lo/Lo nerves identifies Sox2 as an inhibitor of Schwann cell differentiation and myelination. *Proc. Natl. Acad. Sci. USA* **102**, 2596-2601.

Losada, A., Yokochi, T. and Hirano, T. (2005). Functional contribution of Pds5 to cohesin-mediated cohesion in human cells and Xenopus egg extracts. *J. Cell Sci.* **118**, 2133-2141.

Maffini, M. V., Geck, P., Powell, C. E., Sonnenschein, C. and Soto, A. M. (2002). Mechanism of androgen action on cell proliferation: AS3 protein as a mediator of proliferative arrest in the rat prostate. *Endocrinology* **143**, 2708-2714.

Maher, J. F. and Nathans, D. (1996). Multivalent DNA-binding properties of the HMG-1 proteins. *Proc. Natl. Acad. Sci. USA* **93**, 6716-6720.

McLaren, A. (2000). Germ and somatic cell lineages in the developing gonad. *Mol. Cell. Endocrinol.* **163**, 3-9.

Musio, A., Selicorni, A., Focarelli, M. L., Gervasini, C., Milani, D., Russo, S., Vezzoni, P. and Larizza, L. (2006). X-linked Cornelia de Lange syndrome owing to SMC1L1 mutations. *Nat. Genet.* **38**, 528-530.

Nasmyth, K. and Haering, C. H. (2005). The structure and function of SMC and kleisin complexes. *Annu. Rev. Biochem.* **74**, 595-648.

Naughton, C. K., Jain, S., Strickland, A. M., Gupta, A. and Milbrandt, J. (2006). Glial cell-line derived neurotrophic factor-mediated RET signaling regulates spermatogonial stem cell fate. *Biol. Reprod.* **74**, 314-321.

Neuwald, A. F. and Hirano, T. (2000). HEAT repeats associated with condensins, cohesins, and other complexes involved in chromosome-related functions. *Genome Res.* **10**, 1445-1452.

Panizza, S., Tanaka, T., Hochwagen, A., Eisenhaber, F. and Nasmyth, K. (2000). Pds5 cooperates with cohesin in maintaining sister chromatid cohesion. *Curr. Biol.* **10**, 1557-1564.

Rollins, R. A., Morcillo, P. and Dorsett, D. (1999). Nipped-B, a Drosophila homologue of chromosomal adherins, participates in activation by remote enhancers in the cut and Ultrabithorax genes. *Genetics* **152**, 577-593.

Rollins, R. A., Korom, M., Aulner, N., Martens, A. and Dorsett, D. (2004).

Drosophila nipped-B protein supports sister chromatid cohesion and opposes the stromalin/Scc3 cohesion factor to facilitate long-range activation of the cut gene. *Mol. Cell. Biol.* **24**, 3100-3111.

Schule, B., Oviedo, A., Johnston, K., Pai, S. and Francke, U. (2005). Inactivating mutations in ESCO2 cause SC phocomelia and Roberts syndrome: no phenotype-genotype correlation. *Am. J. Hum. Genet.* **77**, 1117-1128.

Seitan, V. C., Banks, P., Laval, S., Majid, N. A., Dorsett, D., Rana, A., Smith, J., Bateman, A., Krpic, S., Hostert, A. et al. (2006). Metazoan Scc4 homologs link sister chromatid cohesion to cell and axon migration guidance. *PLoS Biol.* **4**, e242.

Song, H., Lim, H., Paria, B. C., Matsumoto, H., Swift, L. L., Morrow, J., Bonventre, J. V. and Dey, S. K. (2002). Cytosolic phospholipase A2alpha is crucial [correction of A2alpha deficiency is crucial] for 'on-time' embryo implantation that directs subsequent development. *Development* **129**, 2879-2889.

Svaren, J., Ehrig, T., Abdulkadir, S. A., Ehrengruber, M. U., Watson, M. A. and Milbrandt, J. (2000). EGR1 target genes in prostate carcinoma cells identified by microarray analysis. *J. Biol. Chem.* **275**, 38524-38531.

Tanaka, K., Hao, Z., Kai, M. and Okayama, H. (2001). Establishment and maintenance of sister chromatid cohesion in fission yeast by a unique mechanism. *EMBO J.* **20**, 5779-5790.

Tonkin, E. T., Wang, T. J., Lisgo, S., Bamshad, M. J. and Strachan, T. (2004). NIPBL, encoding a homolog of fungal Scc2-type sister chromatid cohesion proteins and fly Nipped-B, is mutated in Cornelia de Lange syndrome. *Nat. Genet.* **36**, 636-641.

van Heemst, D., James, F., Poggeler, S., Berteaux-Lecellier, V. and Zickler, D. (1999). Spo76p is a conserved chromosome morphogenesis protein that links the mitotic and meiotic programs. *Cell* **98**, 261-271.

Vega, H., Waisfisz, Q., Gordillo, M., Sakai, N., Yanagihara, I., Yamada, M., van Gosliga, D., Kayserili, H., Xu, C., Ozono, K. et al. (2005). Roberts syndrome is caused by mutations in ESCO2, a human homolog of yeast ECO1 that is essential for the establishment of sister chromatid cohesion. *Nat. Genet.* **37**, 468-470.

Vrouwe, M. G., Elghalbzouri-Maghrani, E., Meijers, M., Schouten, P., Godthelp, B. C., Bhuiyan, Z. A., Redeker, E. J., Mannens, M. M., Mullenders, L. H., Pastink, A. et al. (2007). Increased DNA damage sensitivity of Cornelia de Lange syndrome cells: evidence for impaired recombinational repair. *Hum. Mol. Genet.* **16**, 1478-1487.

Wang, F., Yoder, J., Antoshechkin, I. and Han, M. (2003). Caenorhabditis elegans EVL-14/PDS-5 and SCC-3 are essential for sister chromatid cohesion in meiosis and mitosis. *Mol. Cell. Biol.* **23**, 7698-7707.

Wang, S. W., Read, R. L. and Norbury, C. J. (2002). Fission yeast Pds5 is required for accurate chromosome segregation and for survival after DNA damage or metaphase arrest. *J. Cell Sci.* **115**, 587-598.

Watrin, E., Schleiffer, A., Tanaka, K., Eisenhaber, F., Nasmyth, K. and Peters, J. M. (2006). Human Scc4 is required for cohesin binding to chromatin, sister-chromatid cohesion, and mitotic progression. *Curr. Biol.* **16**, 863-874.

Wellik, D. M. and Capecchi, M. R. (2003). Hox10 and Hox11 genes are required to globally pattern the mammalian skeleton. *Science* **301**, 363-367.